Journal of Applied Physics ARTICLE pubs.aip.org/aip/jap

Magnetization characteristics of HTS-stacked ring magnets with and without HTS stack inserts

Cite as: J. Appl. Phys. **134**, 083902 (2023); doi: 10.1063/5.0165643
Submitted: 29 June 2023 · Accepted: 12 August 2023 ·
Published Online: 24 August 2023

Hengpei Liao,[1] Anthony R. Dennis,[2] Weijia Yuan,[1] and Min Zhang[1,a)]

AFFILIATIONS

[1]Applied Superconductivity Laboratory, Department of Electronics and Electrical Engineering, University of Strathclyde, Glasgow G1 1XQ, United Kingdom
[2]Department of Engineering, University of Cambridge, Trumpington Street, Cambridge CB2 1PZ, United Kingdom

[a)]**Author to whom correspondence should be addressed:** min.zhang@strath.ac.uk

ABSTRACT

High-temperature superconducting (HTS) trapped field magnets can generate and maintain stable, high magnetic fields without requiring external power supplies. Recently, HTS-stacked ring magnets have garnered significant attention due to their flexible geometry, robust mechanical strength, and proven trapped field performance. In this study, we examine the magnetization characteristics of HTS-stacked ring magnets and observed a trapped field higher than the applied field during field cooling magnetization. We also observed that by inserting HTS stacks into the hollow cavity of the HTS-stacked rings, the center field ceased to exhibit an increased center field. Our analysis revealed that the unique induced current distribution and the penetration sequence are the underlying causes. Inspired by the investigation results, we explored deeper into the magnetization properties and identified that a final trapped field higher than the applied field can be achieved through proper design and magnetization of the HTS-stacked ring magnets. However, even though the trapped central field experiences an increase, this does not translate into an increment in the total trapped flux. Instead, a redistribution of the flux is observed. These findings hold significant implications for the design and application of superconducting magnets.

I. INTRODUCTION

Trapped field high-temperature superconducting (HTS) magnets are widely investigated for applications such as nuclear magnetic resonance (NMR), HTS machines, and Maglev, which require high and stable magnetic fields.[1–8] Due to the zero resistance under the critical temperature, HTS materials can maintain their current once magnetized. While HTS bulk materials based on ReBCO (Re: rare earth) have been thoroughly studied for their ability to trap more than 17 T,[9–11] HTS stacks based on short HTS tapes have recently garnered attention by achieving even higher trapped fields than those of HTS bulks.[12–14] However, the size and mechanical strength issues still restrict the application of HTS bulk materials, and the HTS stacks also face size limitations.[15–17] Recent observations show trapped fields in hydrides with near-room-temperature critical temperatures under high pressures. These findings offer new insights for trapped field superconductor research. Yet, high-pressure challenges hinder practical applications.[18–20]

HTS ring magnets with persistent current loops in HTS tapes offer a flexible and attractive option for the large-size HTS trapped field magnet design. In contrast to HTS bulks and stacks, HTS ring magnets produced with long commercial 2G HTS tapes can be made in various sizes.[21–27] The feasibility of fabricating jointless tape-based HTS magnets with persistent current was first demonstrated with a single long HTS tape using the "wind-and-flip" method. However, the flip process and long ends of this design make it mechanically weak.[21] To achieve a large and strong magnetic field, our group proposed a new HTS trapped field ring magnet design in 2017 by stacking split HTS tapes and creating a hollow cylinder in the middle.[24] Inspired by the outcomes of this study, we further investigated the trapped field performance under lower temperatures and a 200-layer double-stacked HTS ring magnet with wax impregnation achieved a trapped field of 4.6 T in 2020.[27] To optimize spatial utilization and further enhance trapped, the idea of filling the central space with additional HTS materials came naturally. Shi *et al.* studied the field distribution of a hybrid

ring composed of a ring-shaped magnet and a hollow Bi-2223 tube. The results demonstrated that the declination could be effectively compensated by adjusting the positioning of the Bi-2223 tube.[26] Sheng *et al.* proposed hybridizing round HTS stacks with HTS-stacked rings and "wind-and-flip" coils, respectively, to increase the overall magnet size and magnetic field strength.[25] Both pulsed field magnetization (PFM) and persistent current switch (PCS) were studied for the hybrid samples, demonstrating the feasibility of the concepts. However, these studies of hybrid HTS ring magnets were conducted at 77 K with low fields and a small number of tapes. To investigate the capability of hybrid HTS ring magnets with a higher trapped field as well as the magnetization mechanism of the hybrid HTS-stacked ring magnets, our group demonstrated a novel hybrid HTS-stacked ring magnet with two small HTS bulks in the center of the ring magnets. The hybrid magnet was magnetized to a level of 7.35 T through field cooling[28] and a two-stage magnetization process was verified.

In this study, we further studied the magnetization characteristics of HTS-stacked ring magnets and observed a distinct center field ascent during the field cooling (FC) magnetization process, which was not observed when HTS stacks were inserted. An in-depth investigation was conducted with numerical simulation to figure out the mechanisms driving field ascent and the difference between the sample with and without inserts. It revealed that the unique field penetration sequence and induced current distribution in the HTS-stacked rings play an important role in the center field rising. Based on our findings, we carried out a further study into the magnetization characteristics of HTS-stacked ring magnets with and without HTS stack inserts and uncovered the possibility of achieving a trapped field higher than the initially applied field by the FC process. 2D models were employed to further explain the field ascent from the perspective of magnetic flux and field distribution. This finding and study hold considerable implications for the design and application of HTS trapped field magnets, especially in how to more effectively achieve trapped fields under limited external field conditions.

II. SAMPLE PREPARATION

An HTS-stacked ring magnet was fabricated using a newly designed sample holder capable of providing mechanical support while holding HTS stacks and sensors, as shown in Fig. 1. The two-layer HTS-stacked rings are fabricated with 12 mm Fujikura FESC-SCH tapes, with each layer consisting of 80 HTS tapes. The two HTS stacks are made with 12 mm S-Innovations tapes, featuring a 10–15 μm PbSn coating on two sides. Each stack comprises 90 cut tapes, each measuring 20 mm in length and 12 mm in width. As depicted in Fig. 1, the completed hybrid HTS ring magnet has a length of 83 mm and a width of 46 mm, constrained by the bore size of the magnetization magnet. A Lakeshore HGT-2101 hall sensor (H1) is in the center of the sample. A 1 mm-thick PCB with 10 Hall sensors (H2–H11) is attached to the bottom of the sample holder, and two Cernox SD temperature sensors are fixed at the cover and center of the sample, as shown in Fig. 2. All the sensors have been calibrated. The sample holder's bottom is 2 mm thick, and the Hall sensors are also 2 mm thick, so the trapped fields are measured at a distance of 5 mm above the sample. The finished sample is shown in Fig. 3.

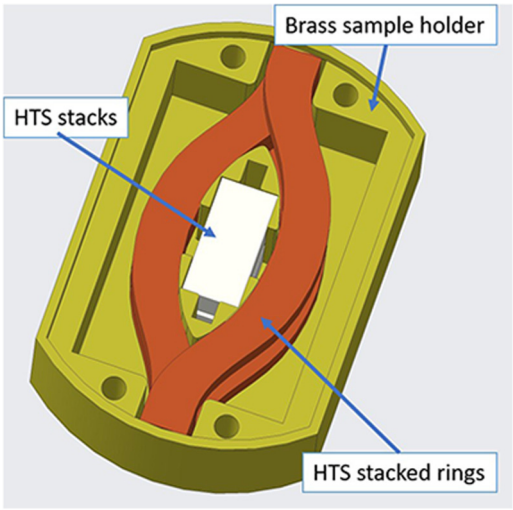

FIG. 1. Scheme of the HTS-stacked ring magnet samples.

III. EXPERIMENTS AND RESULTS

An ICE 12 T wide bore magnet was used to magnetize the sample through a field cooling (FC) process. To minimize temperature rise during magnetization, the field ramping down rate was set at 0.075 T/min, and the cooling power for the sample was adjusted in real-time to maintain the temperature at around 25 K. First, the HTS-stacked ring magnet, without HTS stack inserts, was magnetized using a 4.5 T applied field. Then, the sample was measured two more times: once with the HTS stacks inserted in the center and an applied field of 5 T, and a second time with an increased applied field of 8.5 T. Between each magnetization, the sample was heated to 100 K to quench.

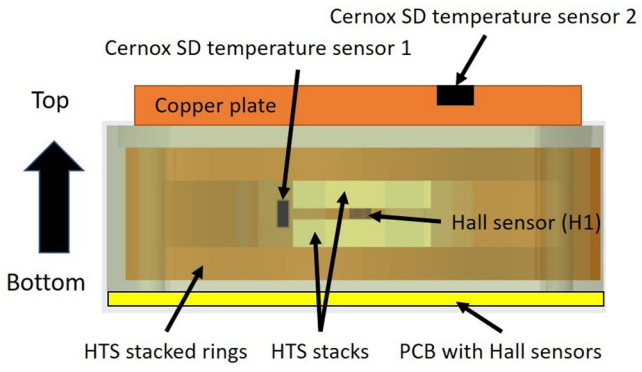

FIG. 2. Arrangement of the sensors.

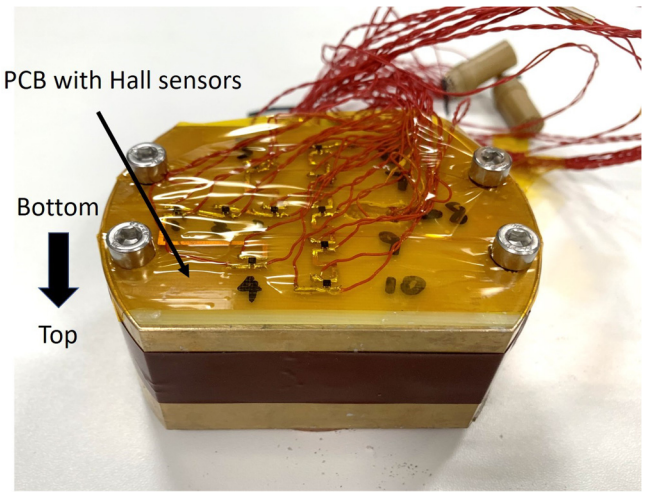

FIG. 3. The finished sample.

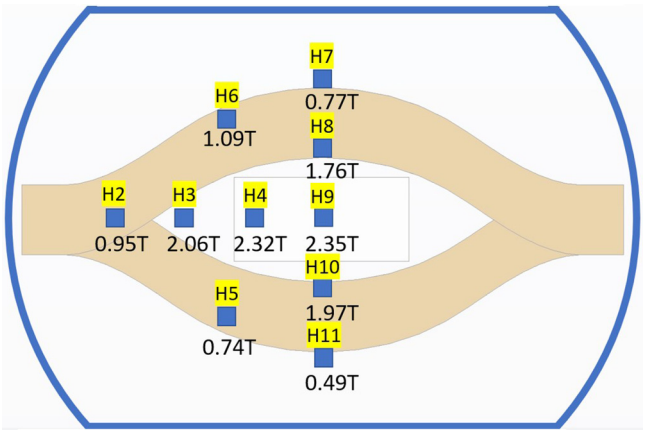

FIG. 5. Trapped field distribution at 5 mm above the HTS-stacked rings under 4.5 T applied field.

As shown in Fig. 4, the center field of the HTS-stacked rings during magnetization was measured with an applied field of 4.5 T. After a 15 min flux creep, the trapped field at the center is 3.79 T, and the fields at 5 mm above are shown in Fig. 5. The curve of sensor H1 exhibited an obvious ascent followed by a subsequent descent until the end of magnetization. This finding suggests that the combination of the center field trapped by the HTS-stacked rings and the external field surpassed the initially applied field, an intriguing phenomenon not observed in previous magnetization tests of HTS trapped field magnets. The field curves for H2–H11 did not show such movement. The temperatures at the center and cover of the sample are shown in Fig. 6. During magnetization, both temperature sensors exhibit a minor temperature increase, however, this increment is less than one degree. Such a minimal rise in temperature is unlikely to significantly impact the properties of the Hall sensor. The temperature of the cover is found to be higher than that at the center, primarily due to the cold helium gas that cools the sample from the bottom, consequently establishing a temperature gradient from the bottom to the top of the sample.

To further explore this field ascent phenomenon, the sample was inserted with HTS stacks and magnetized again. As shown in Fig. 7, the field at the center of the sample stayed stable until the end of magnetization with a 5 T applied field which indicated the hybrid sample may not be fully penetrated. Then, the applied field

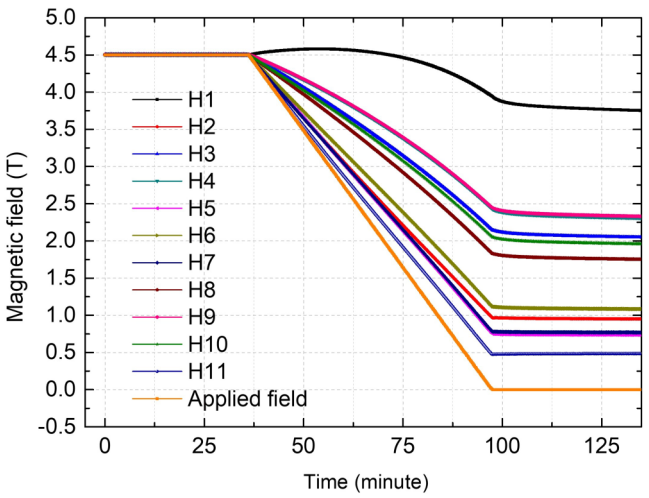

FIG. 4. Field values during the magnetization of HTS-stacked rings with 4.5 T applied field.

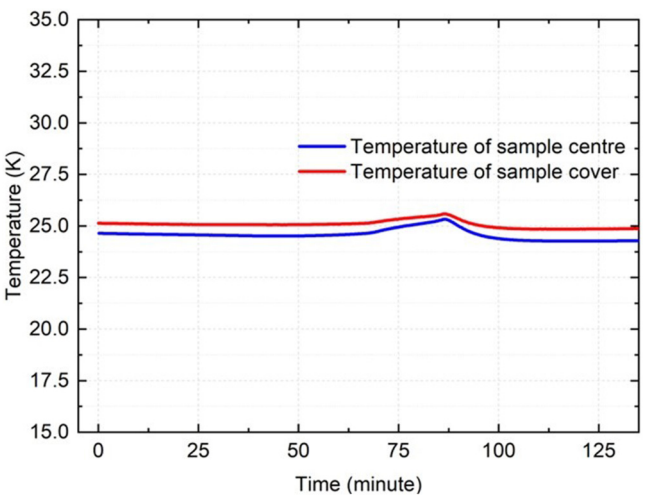

FIG. 6. Temperatures of the cover and center of the sample during 4.5 T magnetization.

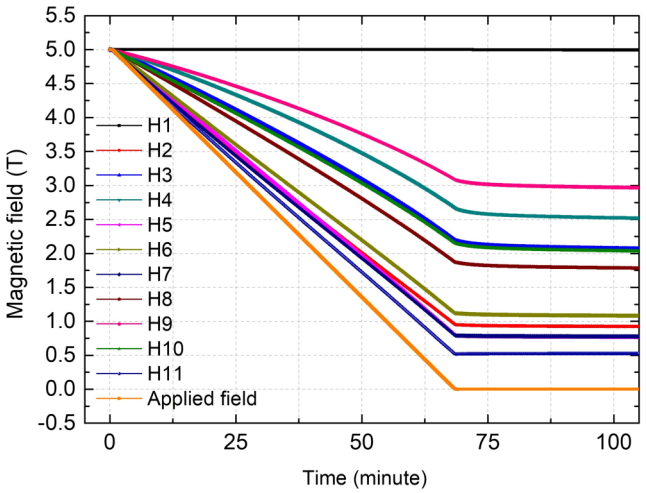

FIG. 7. Field values during 5 T FC magnetization of the hybrid HTS-stacked ring magnet.

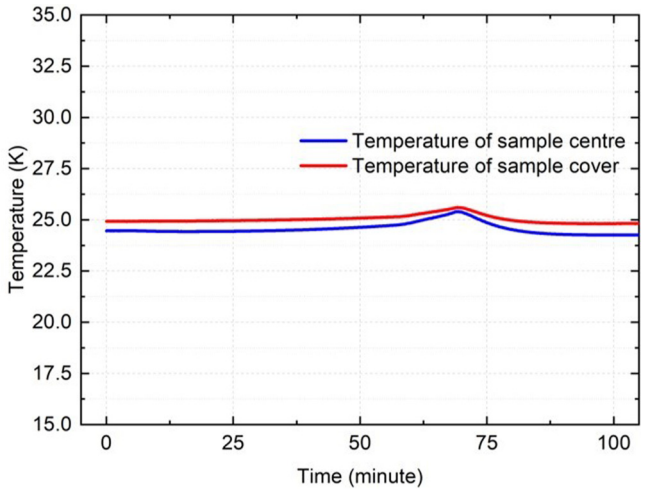

FIG. 9 Temperatures of the cover and center of the sample during 5 T magnetization.

for magnetization was increased to 8.5 T and the field curves are depicted in Fig. 8. At elevated magnetic fields, the hybrid sample manifested indications of full penetration with a decrease in the center field before the end of magnetization. The final center trapped field is 6.6 T and no upward trend was observed throughout the entire process. The fields at H2–H11 positions exhibit the same ramping-down trends for both magnetization tests. As demonstrated in Figs. 9 and 10, a similar rise in temperature occurs during both the 5 and 8.5 T magnetization processes. This confirms that the ascension of the central field in the 4.5 T magnetization of the HTS-stacked ring magnet is not due to temperature fluctuations.

In light of the above experimental tests, one may infer that the existence of HTS stack inserts can affect the observed center field ascending trend in the HTS-stacked rings. This finding has sparked interest because it suggests that the HTS-stacked rings possess magnetization characteristics distinct from the other HTS trapped field magnets. This characteristic may potentially have significant implications for the design of HTS trapped field magnets and will be studied further with numerical models.

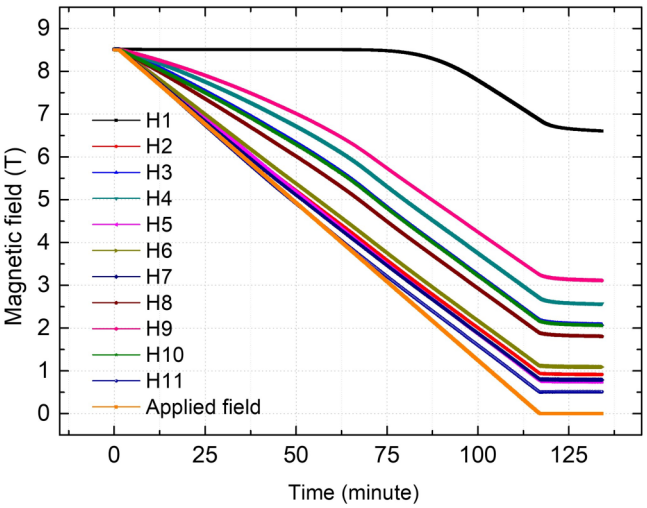

FIG. 8. Field values during 8.5 T FC magnetization of the hybrid HTS-stacked ring magnet.

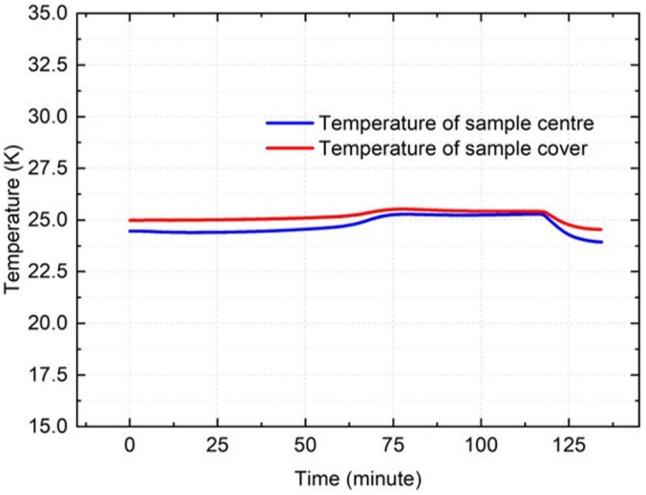

FIG. 10. Temperatures of the cover and center of the sample during 8.5 T magnetization.

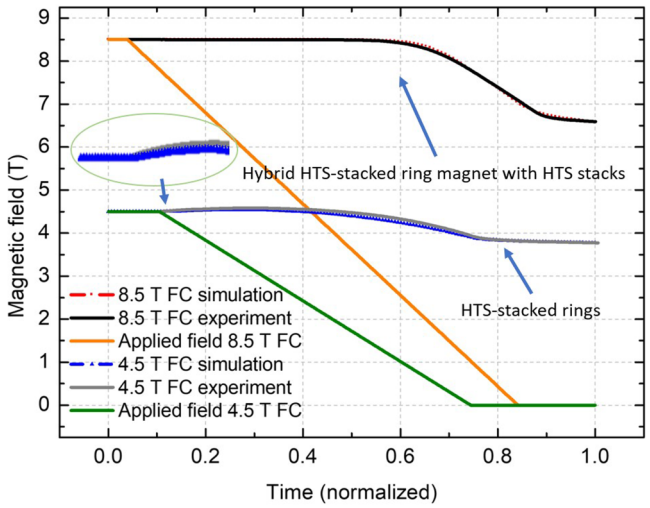

FIG. 11. Center field at the samples during magnetizations.

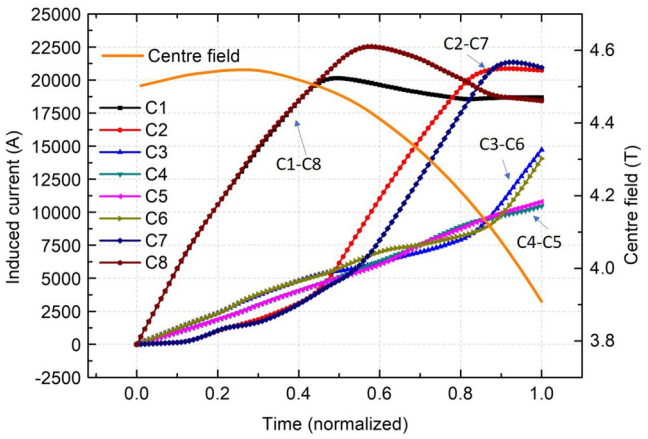

FIG. 13. Induced currents at each domain of HTS-stacked rings and center field during magnetization.

IV. SIMULATION AND DISCUSSION

To further investigate the underlying reason for this phenomenon, a comprehensive numerical study was conducted to evaluate the current, penetration, and field distributions of the hybrid magnet during the magnetization process. To this end, a 3D numerical model was developed based on the homogenized H formulation using Comsol Multiphysics.[25] The governing equation for this model is given by Eq. (1),

$$\mu_0\mu_r\frac{\partial H}{\partial t}+\nabla\times(\rho\nabla\times H)=0, \tag{1}$$

$$\rho=\frac{E_0}{Jc(\theta,B)}\times\left(\frac{J}{Jc(\theta,B)}\right)^{n-1}, \tag{2}$$

where magnetic field intensity $H=[H_x, H_y, H_z]$ are the variables. ρ is the resistivity of HTS materials. The relative permeability μ_r is assumed to be 1 for substrate layers and copper stabilizers which are non-magnetic materials. ρ is deduced from the E–J power law as shown in Eq. (2). E_0 is the critical current criterion equal to 100 μV/m and n is the power law exponent which is set as 21. In the numerical model, the magnetic field dependence of critical current density $J_c(\theta, B)$ is considered using direct interpolation of measurements at 25 K for both Fujikura tapes and S-Innovations

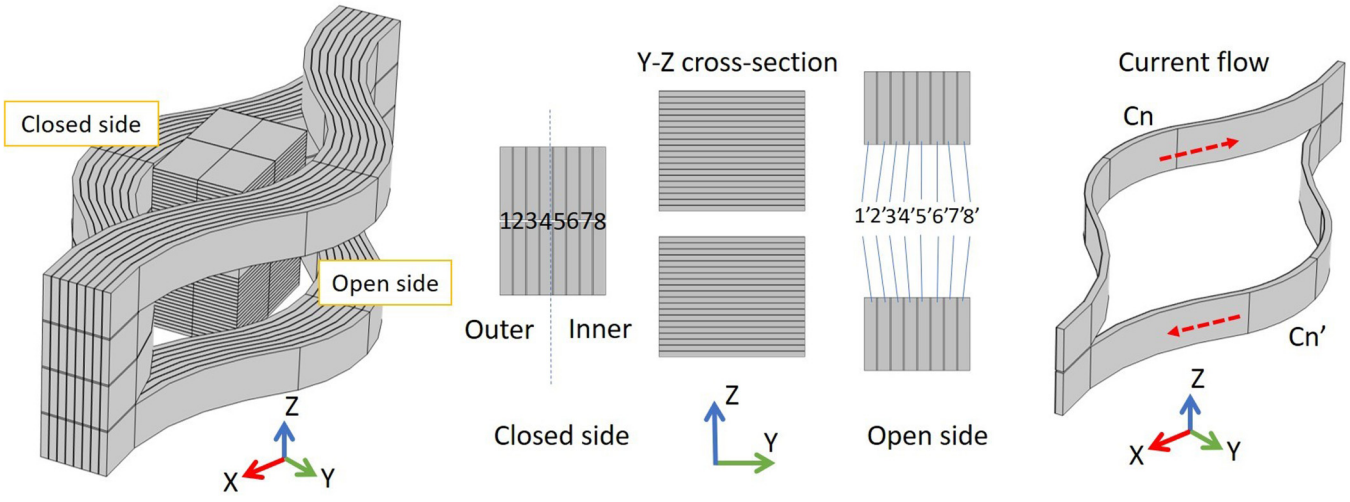

FIG. 12. Scheme of the homogenized model for the hybrid HTS-stacked ring magnet.

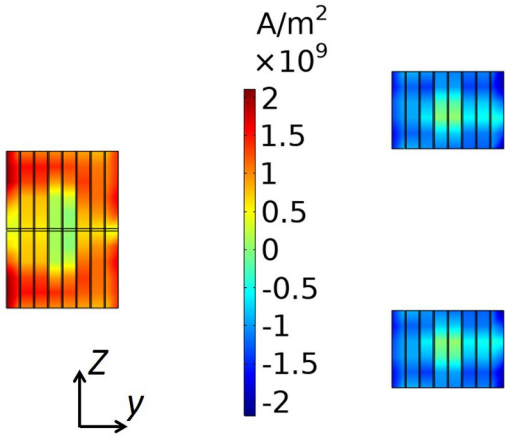

FIG. 14. Induced current density of the HTS-stacked rings.

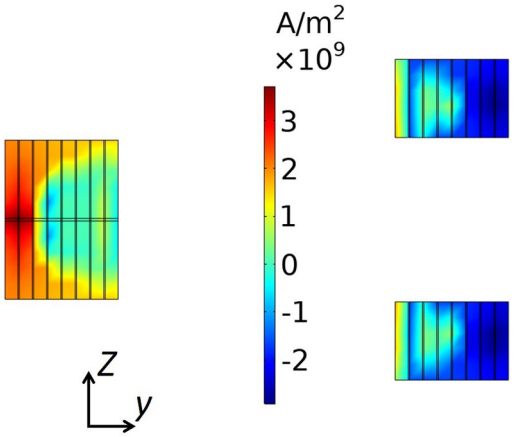

FIG. 16. Induced current density of the ring-shaped HTS bulk material.

tapes. Homogenization is utilized to expedite the calculation, where 10 tapes are homogenized into one domain for the HTS-stacked rings, while 5 short tapes are represented by one domain for the HTS stacks. The field cooling condition is simulated by regulating the applied field using the Dirichlet boundary condition. As the actual field ramping rate is relatively slow, and the associated temperature change is minimal, the model does not consider heat generation.

To verify the accuracy of the numerical model, the trapped fields obtained through both experiments and simulations are compared in Fig. 11. It reveals good agreement between the two results, including the center field ascent of the HTS-stacked rings, which will be discussed in detail later. In Fig. 12, a schematic diagram of the cross section of the hybrid HTS magnet is presented. The closed side and open side are used to refer to the two sides of the HTS-stacked rings, according to the shape. The numbers correspond to combinations of the upper and lower domains, with each domain comprising 10 HTS tapes.

The investigation begins with the induced current at each domain during the magnetization process of the HTS-stacked rings with 4.5 T applied field. As illustrated in Figs. 13 and 14, the induced currents from 1 to 8 domains are presented by Cn. As the rings are constructed using split tapes, Cn and Cn′ should theoretically be identical, representing currents within the same loop. Therefore, we have not included a separate discussion on Cn′. It can be observed that C1–C8, C2–C7, C3–C6, and C4–C5 exhibit similar values and trends during the magnetization, respectively. The innermost rings (C8) have almost the same induced current as

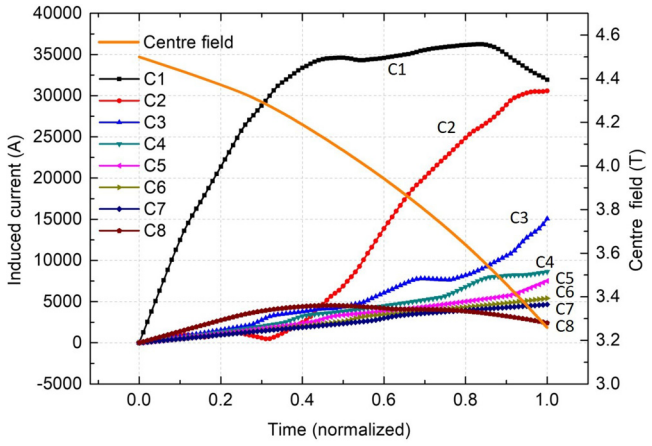

FIG. 15. Induced currents at each domain of ring-shaped HTS bulk material and center field during magnetization.

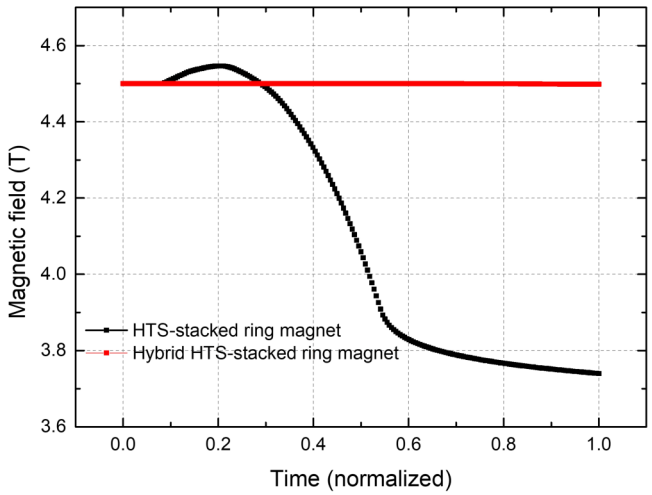

FIG. 17. Center field of the HTS-stacked ring magnet with and without HTS stack inserts.

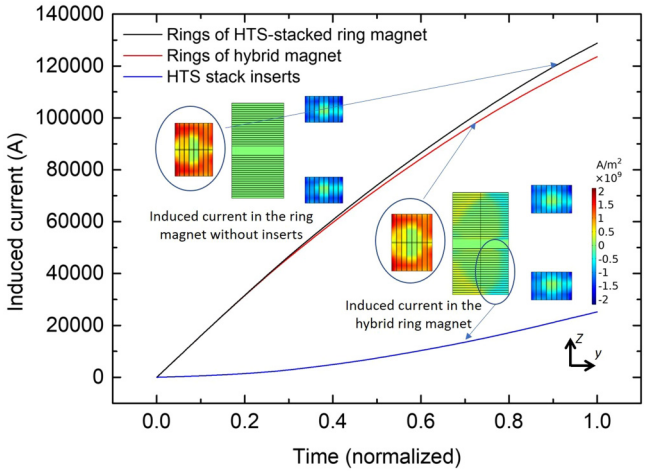

FIG. 18. Total induced current in the HTS-stacked rings and the induced current in the HTS stacks.

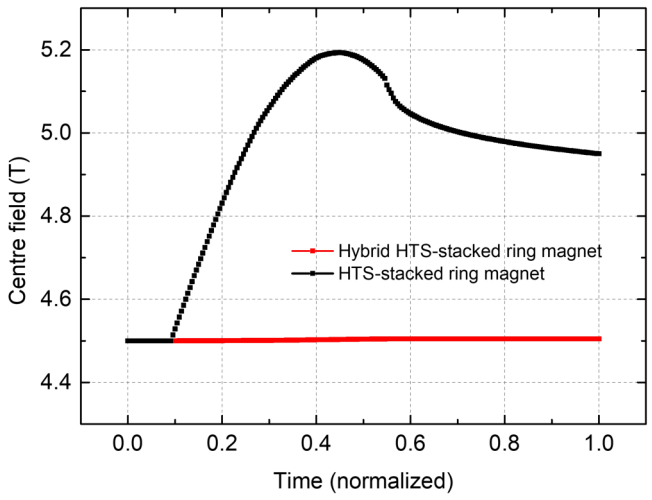

FIG. 20. Center field of the double-turn HTS-stacked ring magnets with and without HTS stack inserts.

the outermost rings (C1), especially at the end of magnetization, owing to the parallel stacking method employed in the HTS-stacked rings. The difference between C1–C8, C2–C7, C3–C6, and C4–C5 is considered to be influenced by the asymmetry of the geometry and the trapped field of the HTS-stacked rings. If there is only one layer of HTS-stacked rings, the induced currents should be symmetrically equal from the inside out in theory.

The field penetration is revealed in Fig. 14. The inner and outer domains are simultaneously penetrated toward the middle domains, which is consistent with the induced current curves. For comparison, an alternative model is built in which the HTS bulk material with the same geometry as HTS-stacked rings is employed. As shown in Fig. 15, the induced current is lower in the inner domains which means they are less penetrated, and the center field does not rise during the magnetization process. The final trapped field by the HTS bulk ring is slightly lower. The HTS bulk material is penetrated from the outer domains to the inner domains, which agrees with the traditional penetration rule as illustrated in Fig. 16. Based on this comparative study, we can conclude that the penetration sequence and the associated current distribution are the causes of this unique center field ascent.

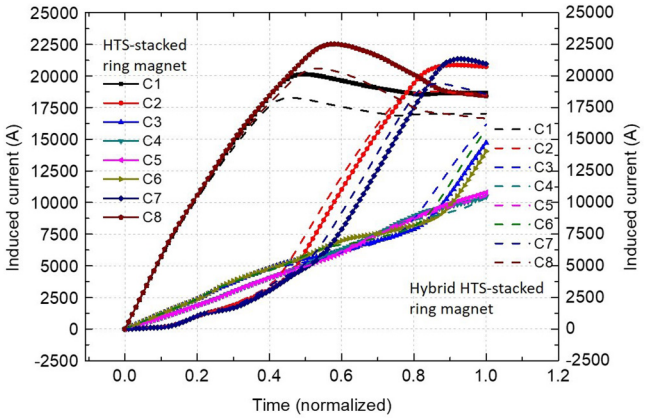

FIG. 19. Induced current in each domain of HTS-stacked rings.

As it is mentioned above, with the presence of the HTS stacks, the field in the center ceases to rise during magnetization. To figure out the reason, we calculated the hybrid HTS-stacked ring magnet with a 4.5 T applied field for a comparative study. The center field of the hybrid magnet exhibits the same stable value as shown in Fig. 17. The total induced current in the HTS-stacked rings, as well as that in half of the HTS stacks, are illustrated in Fig. 18. In the case of a hybrid design, the total induced current within the rings is slightly reduced, and there is induced current shared in the HTS stacks during the magnetization. Due to the asymmetric field of HTS-stacked rings, the HTS stacks are penetrated asymmetrically in the z-x plane and symmetrically in the z-y plane,[25] but it still follows the penetration law of ordinary HTS materials, i.e., the penetration occurs from the outside to the inside. Figure 19 provides a more direct representation that the induced current within the innermost domains, which has the greatest impact on the center field, is noticeably reduced due to the presence of HTS stack inserts. In brief, the two factors, reduced current in the inner domains and HTS stacks sharing current, are the reasons why the hybrid sample did not see the center field ascent.

Based on the above analysis, we figured out that the unique parallel stacking method, which makes the induced currents of the inner domains approximately equal to those of the outer domains, drives the center field rising during magnetization. The existence of HTS stack inserts that reduced and share the induced current in the rings can suppress this phenomenon. However, the analysis pushed us to consider what would happen to the center field, if the

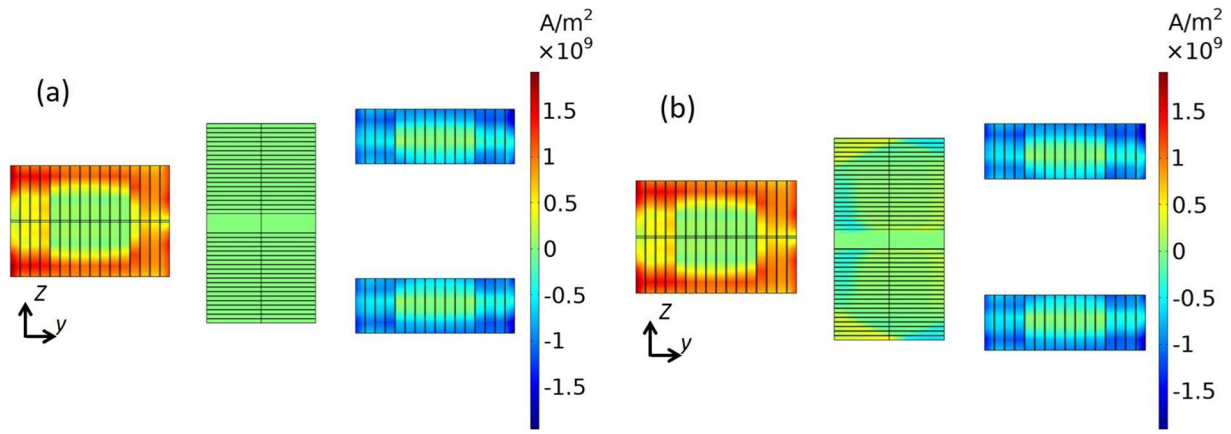

FIG. 21. Induced current density of the double-turn HTS magnet. (a) HTS-stacked ring magnet and (b) hybrid HTS-stacked ring magnet.

HTS-stacked rings have more turns and larger sizes. It is important to note that increasing the number of turns in HTS ring magnets results in an increased length, which surpasses the limitations of the wide bore magnet. Consequently, the subsequent investigation is primarily based on numerical simulations. By doubling the turns for the HTS-stacked rings and keeping the width of the central space unchanged, we conducted a thorough examination of the magnetization characteristics.

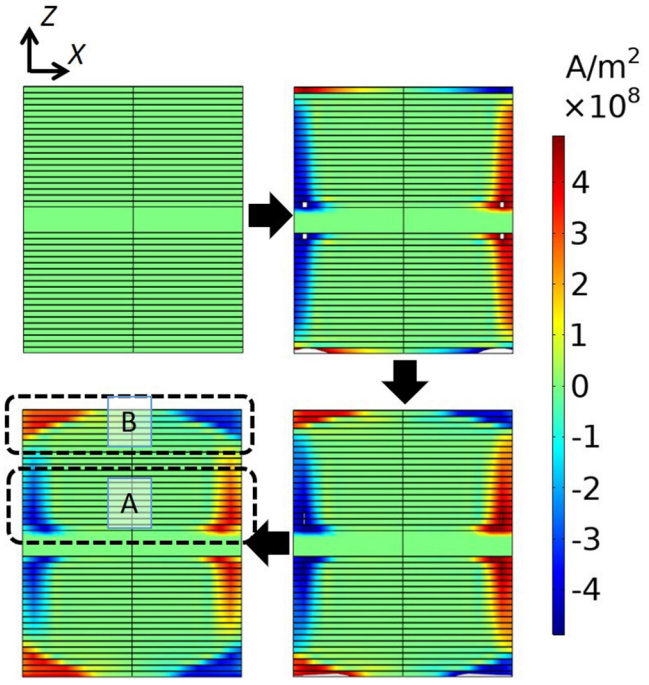

FIG. 22. Penetration of the z–x cross section of the HTS stacks during magnetization.

Figure 20 illustrates the center field during 4.5 T magnetization of the doubled HTS-stacked rings. The center field keeps ramping up until it peaks before the end of magnetization. The highest achieved field is 5.2 T and the final field markedly exceeds the applied field by around 0.4 T, which is a feat that cannot be achieved by HTS bulks or stacks alone. The center field of the hybrid one does not exhibit such an increase, but a stable straight line. These results reveal the possibility of achieving a trapped field which is higher than the applied field with HTS-stacked ring magnets.

The field penetration in Fig. 21 indicates that the rings of both models are far from fully penetrated and the current is mainly induced in the innermost and outermost domains at the end of magnetization. However, Fig. 22 depicts the current distribution in the z-x cross section which shows the penetration pattern of the HTS stacks is partially magnetized reversely. The induced current

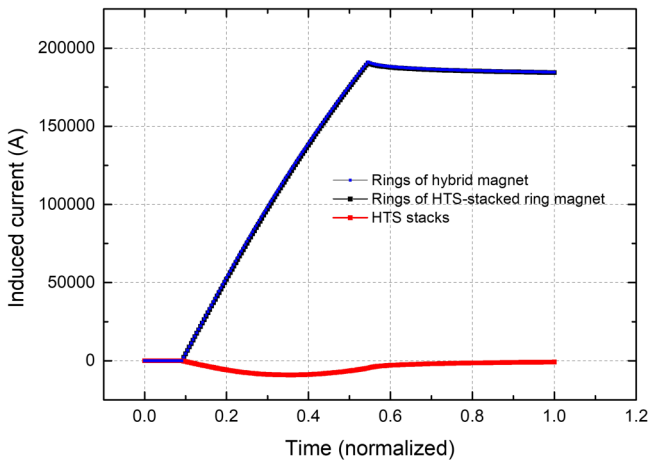

FIG. 23. The total induced current within ring domains and HTS stack domains.

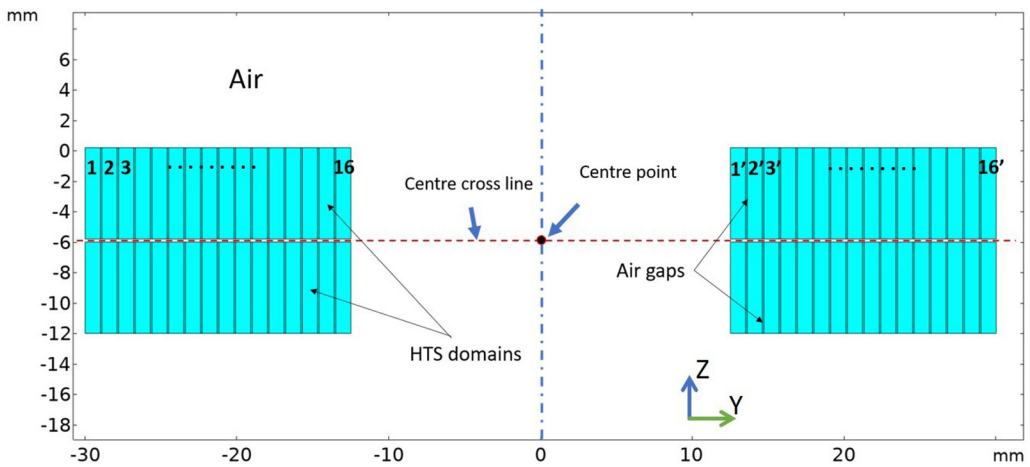

FIG. 24. 2D HTS-stacked ring models with infinite length.

directions in regions A and B are opposite and evident. As area A is located closer to the center where the field would experience an ascending trend in the absence of HTS stacks, the induced current in this area serves to prevent the field from increasing.

The total induced currents in the ring domains and stack domains are illustrated in Fig. 23. The induced current in the ring domains is similar for both models. However, the HTS stack model exhibits the induction of a reverse current, which is consistent with the analysis of current distribution in the HTS stacks. This reverse current serves to suppress the ascending trend of the center field.

To obtain a comprehensive understanding of the field ascent phenomenon, specifically concerning trapped magnetic flux and field distribution, 2D homogenized models are built. Assuming the infinite length of the HTS-stacked rings, the gap on the open side (as depicted in Fig. 11) can be reduced to match that of the closed side, resulting in the configuration depicted in Fig. 24. Following the parallel stacking method, the induced current within the HTS-stacked rings follows the equation $Cn + Cn' = 0$. As a point of comparison, a model without current restrictions, which behaves like normal HTS bulk material, is also calculated.

The center field profiles of the two models are presented in Fig. 25. While the center field of the HTS-stacked rings continues to rise until the end of magnetization, the center field of the HTS bulk material decreases steadily from the outset of magnetization. This observation further confirms the feasibility of achieving a trapped field that exceeds the applied field. Figure 26 illustrates the

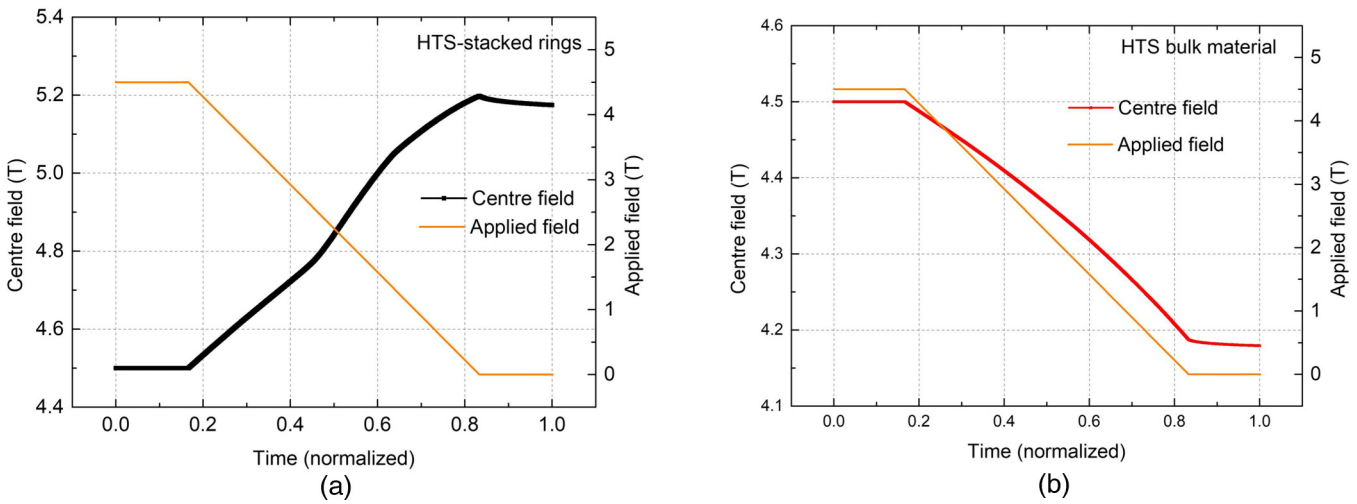

FIG. 25. Center field of the 2D models: (a) HTS-stacked rings. (b) HTS bulk material.

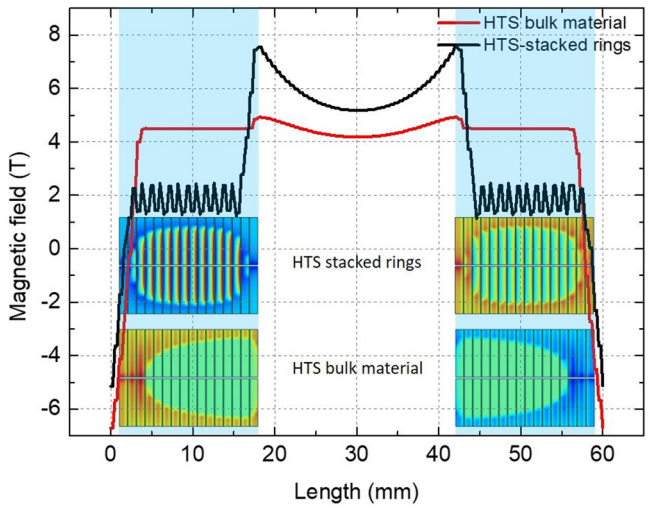

FIG. 26. Final trapped fields at the center cross line.

final trapped field along the y axis direction. Compared to the HTS bulk material, the trapped field of the HTS-stacked rings exhibits a higher center field with a more concave shape in the central area. However, in the HTS material region, the field of the HTS-stacked rings drops rapidly to less than half of its center field, which is attributed to the unique distribution of induced current and penetration sequence. The HTS bulk material, on the other hand, maintains a broad flat field across the HTS area, following the conventional magnetization law of HTS materials.

Figure 27 depicts the change in the y axis magnetic flux across the center cross line. Initially, both models have the same magnetic flux. However, the flux of the HTS-stacked rings decreases more rapidly, resulting in a lower trapped flux along the center cross line. This indicates that even though the HTS-stacked rings can achieve a higher center trapped field, it does not necessarily translate into a higher total trapped flux in the entire center area. The final magnetic energy of the HTS-stacked rings is 15 661 J/m, while that of the HTS bulk material is 16 056 J/m. This result can be explained through the concept of magnetic flux pinching. The higher induced current in the inner HTS domains leads to more flux lines being compressed or concentrated in a specific center area, but the overall flux lines cannot be increased. As a result, the field outside the center area decreases rapidly, as observed in Fig. 26.

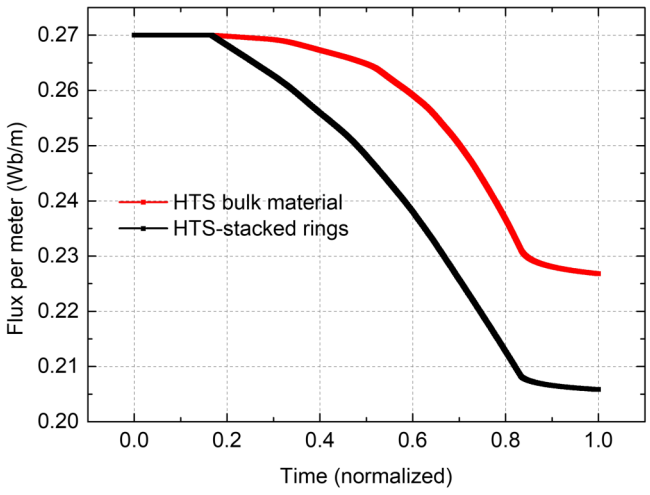

FIG. 27. Magnetic flux through the center cross line during magnetization.

V. SUMMARY

This study presents an in-depth investigation of tape-based HTS-stacked ring magnets, revealing a unique field ascent phenomenon during magnetization that can be avoided through the use of HTS stack inserts. Numerical simulations show that the higher current induced in the inner domains of the HTS-stacked rings causes the center field ascent, while the HTS stacks can reduce the current in the inner domains, preventing the center field from rising. Additionally, by doubling the turns of the HTS-stacked rings, a trapped field higher than the initially applied field can be achieved with field cooling magnetization. This characteristic is unique to HTS-stacked ring magnets and has not been found in other HTS trapped field magnets. Furthermore, HTS stack inserts can be induced with reverse currents to maintain the center field during magnetization. Despite achieving a higher center field, the trapped flux of HTS-stacked ring magnets is not higher than that of the similarly sized HTS bulk material, as demonstrated by an analysis of the trapped field distribution and magnetic flux variation.

ACKNOWLEDGMENTS

This research was supported by the Royal Academy of Engineering Research Fellowship for Professor Min Zhang. The authors would like to acknowledge the Henry Royce Institute (Equipment Grant Ref. No. EP/P024947/1) for financial support. The authors would like to thank the Cambridge Bulk Group for their technical support during testing.

AUTHOR DECLARATIONS

Conflict of Interest

The authors have no conflicts to disclose.

Author Contributions

Hengpei Liao: Conceptualization (equal); Data curation (equal); Formal analysis (equal); Investigation (equal); Methodology (equal); Project administration (equal); Resources (equal); Software (equal); Validation (equal); Visualization (equal); Writing – original draft (equal); Writing – review & editing (equal). **Anthony Dennis:** Data curation (equal); Software (equal). **Weijia Yuan:** Funding acquisition (equal); Methodology (equal); Resources (equal); Supervision (equal). **Min Zhang:** Conceptualization (equal); Formal analysis (equal); Funding acquisition (equal);

Investigation (equal); Project administration (equal); Supervision (equal); Writing – review & editing (equal).

DATA AVAILABILITY

The data that support the findings of this study are available from the corresponding author upon reasonable request.

REFERENCES

[1]T. Kii, R. Kinjo, N. Kimura, M. Shibata, M. A. Bakr, Y. W. Choi, M. Omer, K. Yoshida, K. Ishida, T. Komai, K. Shimahashi, T. Sonobe, H. Zen, K. Masuda, and H. Ohgaki, IEEE Trans. Appl. Supercond. **22**, 4100904 (2012).
[2]T. Nakamura, Y. Itoh, M. Yoshikawa, T. Oka, and J. Uzawa, Concepts Magn. Reson. Part B **31B**, 65 (2007).
[3]Z. Deng, W. Zhang, J. Zheng, B. Wang, Y. Ren, X. Zheng, and J. Zhang, IEEE Trans. Appl. Supercond. **27**, 1 (2017).
[4]J. H. Durrell, M. D. Ainslie, D. Zhou, P. Vanderbemden, T. Bradshaw, S. Speller, M. Filipenko, and D. A. Cardwell, Supercond. Sci. Technol. **31**, 103501 (2018).
[5]F. N. Werfel, U. Floegel-Delor, R. Rothfeld, T. Riedel, B. Goebel, D. Wippich, and P. Schirrmeister, Supercond. Sci. Technol. **25**, 014007 (2012).
[6]D. Zhou, M. Izumi, M. Miki, B. Felder, T. Ida, and M. Kitano, Supercond. Sci. Technol. **25**, 103001 (2012).
[7]M. Miki, S. Tokura, H. Hayakawa, H. Inami, M. Kitano, H. Matsuzaki, Y. Kimura, I. Ohtani, E. Morita, H. Ogata, M. Izumi, H. Sugimoto, and T. Ida, Supercond. Sci. Technol. **19**, S494–S499 (2006).
[8]Y. Zhang, D. Zhou, T. Ida, M. Miki, and M. Izumi, Supercond. Sci. Technol. **29**, 044005 (2016).
[9]M. Tomita and M. Murakami, Nature **421**, 517–520 (2003).
[10]Y. Shi, D. Kumar Namburi, W. Zhao, J. H. Durrell, A. R. Dennis, and D. A. Cardwell, Supercond. Sci. Technol. **29**, 015010 (2016).
[11]J. H. Durrell, A. R. Dennis, J. Jaroszynski, M. D. Ainslie, K. G. B. Palmer, Y. H. Shi, A. M. Campbell, J. Hull, M. Strasik, E. E. Hellstrom, and D. A. Cardwell, Supercond. Sci. Technol. **27**, 082001 (2014).
[12]A. Patel, S. C. Hopkins, and B. A. Glowacki, Supercond. Sci. Technol. **26**, 032001 (2013).
[13]T. Tamegai, T. Hirai, Y. Sun, and S. Pyon, Physica C **530**, 20–23 (2016).
[14]M. Suyama, S. Pyon, Y. Iijima, S. Awaji, and T. Tamegai, Supercond. Sci. Technol. **35**, 02LT01 (2022).
[15]J. R. Hull and M. Murakami, Proc. IEEE **92**, 1705–1718 (2004).
[16]M. Suyama, S. Pyon, Y. Iijima, S. Awaji, and T. Tamegai, Supercond. Sci. Technol. **34**, 065004 (2021).
[17]A. Patel, A. Baskys, T. M. Williams, A. McCaul, W. Coniglio, J. Hänisch, M. Lao, and B. A. Glowacki, Supercond. Sci. Technol. **31**, 09LT01 (2018).
[18]J. E. Hirsch and F. Marsiglio, Physica C **589**, 1353916 (2021).
[19]V. S. Minkov, V. Ksenofontov, S. L. Bud'ko, E. F. Talantsev, and M. I. Eremets, Nat. Phys. **2023** (2023).
[20]S. K. Goh, W. Zhang, and K. Y. Yip, Nat. Phys. **2023** (2023).
[21]H.-G. Lee, J.-G. Kim, S.-W. Lee, W.-S. Kim, S.-W. Lee, K.-D. Choi, G.-W. Hong, and T.-K. Ko, Physica C: Supercond. Appl. **445–448**, 1099–1102 (2006).
[22]G. A. Levin, P. N. Barnes, J. Murphy, L. Brunke, J. D. Long, J. Horwath, and Z. Turgut, Appl. Phys. Lett. **93**, 062504 (2008).
[23]H. G. Lee, J. G. Kim, S. W. Lee, W. S. Kim, S. W. Lee, K. D. Choi, G. W. Hong, and T. K. Ko, Physica C **445–448**, 1099–1102 (2006).
[24]J. Sheng, M. Zhang, Y. Wang, X. Li, J. Patel, and W. Yuan, Supercond. Sci. Technol. **30**, 094002 (2017).
[25]J. Sheng, Y. Pan, J. Jiang, W. Li, B. Shen, Z. Zhang, and W. Wu, IEEE Trans. Appl. Supercond. **29**, 1–5 (2019).
[26]J. Shi, X. Li, and J. Sheng, IEEE Trans. Appl. Supercond. **32**, 3600605 (2022).
[27]M. Z. Ali, J. Zheng, F. Huber, Z. Zhang, W. Yuan, and M. Zhang, Supercond. Sci. Technol. **33**, 04LT01 (2020).
[28]H. Liao, W. Yuan, Z. Zhang, and M. Zhang, J. Appl. Phys. **133**, 023902 (2023).